Icarus 215 (2011) 547–551

Contents lists available at SciVerse ScienceDirect

Icarus

journal homepage: www.elsevier.com/locate/icarus

Radar observations of Asteroids 64 Angelina and 69 Hesperia

Michael K. Shepard [a,*], Alan W. Harris [b], Patrick A. Taylor [c], Beth Ellen Clark [d], Maureen Ockert-Bell [d], Michael C. Nolan [c], Ellen S. Howell [c], Christopher Magri [e], Jon D. Giorgini [f], Lance A.M. Benner [f]

[a] Bloomsburg University, 400 E. Second St., Bloomsburg, PA 17815, USA
[b] Space Science Institute, La Cañada, CA 91011-3364, USA
[c] NAIC/Arecibo Observatory, HC 3 Box 53995, Arecibo, PR 00612, USA
[d] Ithaca College, Ithaca, NY 14853, USA
[e] University of Maine at Farmington, Farmington, ME 04938, USA
[f] Jet Propulsion Laboratory, Pasadena, CA 91109, USA

ARTICLE INFO

Article history:
Received 8 July 2011
Revised 26 July 2011
Accepted 26 July 2011
Available online 3 August 2011

Keywords:
Asteroids
Asteroids, Composition
Radar observations

ABSTRACT

We report new radar observations of E-class Asteroid 64 Angelina and M-class Asteroid 69 Hesperia obtained with the Arecibo Observatory S-band radar (2480 MHz, 12.6 cm). Our measurements of Angelina's radar bandwidth are consistent with reported diameters and poles. We find Angelina's circular polarization ratio to be 0.8 ± 0.1, tied with 434 Hungaria for the highest value observed for main-belt asteroids and consistent with the high values observed for all E-class asteroids (Benner, L.A.M., Ostro, S.J., Magri, C., Nolan, M.C., Howell, E.S., Giorgini, J.D., Jurgens, R.F., Margot, J.L., Taylor, P.A., Busch, M.W., Shepard, M.K. [2008]. Icarus 198, 294–304; Shepard, M.K., Kressler, K.M., Clark, B.E., Ockert-Bell, M.E., Nolan, M.C., Howell, E.S., Magri, C., Giorgini, J.D., Benner, L.A.M., Ostro, S.J. [2008b]. Icarus 195, 220–225). Our radar observations of 69 Hesperia, combined with lightcurve-based shape models, lead to a diameter estimate, $D_{\rm eff}$ = 110 ± 15 km, approximately 20% smaller than the reported IRAS value. We estimate Hesperia to have a radar albedo of $\hat{\sigma}_{\rm OC} = 0.45 \pm 0.12$, consistent with a high-metal content. We therefore add 69 Hesperia to the Mm-class (high metal M) (Shepard, M.K., Clark, B.E., Ockert-Bell, M., Nolan, M.C., Howell, E.S., Magri, C., Giorgini, J.D., Benner, L.A.M., Ostro, S.J., Harris, A.W., Warner, B.D., Stephens, R.D., Mueller, M. [2010]. Icarus 208, 221–237), bringing the total number of Mm-class objects to eight; this is 40% of all M-class asteroids observed by radar to date.

1. XME-class asteroid properties

The Tholen (1984) X-complex of asteroids is defined by nearly featureless visible and near-infrared spectra. They are subdivided based on optical albedo into P-class ($p_v < 0.1$), M-class ($0.1 \leqslant p_v \leqslant 0.3$), and E-class ($p_v > 0.3$).

The M-class asteroids have been scrutinized by numerous groups and there is strong evidence that individual members are made up of several possible meteoritic classes including irons, stony-irons (pallasites and mesosiderites), enstatite chondrites, and even carbonaceous chondrites (Chapman and Salisbury, 1973; Gaffey, 1976; Gaffey and McCord, 1979; Bell et al., 1989; Lupishko and Belskaya, 1989; Cloutis et al., 1990; Vilas, 1994; Rivkin et al., 2000; Hardersen et al., 2005; Vernazza et al., 2009). Radar observations have been reported for 19 M-class objects and about 40% of the M-class asteroids have radar albedos consistent with dominantly iron compositions (Shepard et al., 2010). Shepard et al. (2010) suggested designating this high radar albedo group the Mm-class (M-class, metallic). The remaining objects have radar albedos suggesting an iron content most consistent with stony-irons, enstatite chondrites, or high-iron exotics such as bencubbinites (Shepard et al., 2008a, 2010).

The E-class asteroids are characterized by high optical albedos, $p_v > 0.3$. Most spectroscopists agree the spectra and albedo of these asteroids indicate an enstatite achondritic (aubrite) composition (Zellner et al., 1977). Recent observations at higher spectral-resolutions suggest the occasional presence of the sulfides troilite and oldhamite and have led to a division into three sub-classes. Using spectra from 0.4 to 2.5 μm, Clark et al. (2004) suggested dividing these into classes based on the major members of the different spectral types: 64 Angelina-type, 44 Nysa-like, and 434 Hungaria-like. Using spectra from 0.4 to 1.0 μm, Gaffey and Kelley (2004) suggest a slightly different division: E[I], lacking any diagnostic absorptions; E[II], characterized by a strong absorption at 0.49 μm and occasionally weaker feature at 0.96 μm; and E[III], characterized by a weak feature at 0.88–0.90 μm. The Gaffey and Kelley (2004) divisions differ from those of Clark et al. (2004) in that Angelina (the subject of this paper) and Hungaria are both considered E[II].

* Corresponding author.
E-mail address: mshepard@bloomu.edu (M.K. Shepard).

0019-1035/$ - see front matter © 2011 Elsevier Inc. All rights reserved.
doi:10.1016/j.icarus.2011.07.027

In this paper, we report on new radar observations of the E-class Asteroid 64 Angelina and the M-class Asteroid 69 Hesperia. These are the latest observations in our long-term radar survey of all E- and M-class asteroids that can be observed by Arecibo, the most powerful astronomical radar system available. Our goals are to better characterize the properties of asteroids belonging to these enigmatic classes, including size, shape, spin state, radar and optical albedos, and composition.

2. Radar observations

Radar observations differ significantly from those made with optical telescopes. Good reviews of methods, techniques, and the analyses of asteroid echoes can be found in Ostro et al. (2002) and references therein. Below we summarize the main points required to understand the results of this paper.

Each radar observing cycle or "run" consists of transmission of a circularly polarized 2380 MHz (12.6 cm) signal for the round-trip light travel time to the target, followed by reception of echoes for a similar duration in the opposite (OC) and same (SC) senses of circular polarization as transmitted. We measure the radar cross-sections of our targets (in km^2) σ_{OC} and σ_{SC}, by integrating the continuous wave (CW) power spectra. These are equivalent to the cross-sectional areas of a smooth, metallic sphere (a perfect reflector) that would generate the observed echo power when viewed at the same distance.

For an asteroid observed at S-band (2380-MHz), its apparent width, D (in km) normal to the apparent spin vector at rotation phase φ, is related to the instantaneous bandwidth B (in Hz) of the radar echo (due to the apparent rotation), the target's physical properties, and its orientation by

$$D(\phi) = \frac{PB(\phi)}{27.7\cos\delta} \quad (1)$$

where P is the apparent (synodic) rotation period in hours and δ is the sub-radar latitude. For each target we estimate the minimum bandwidth and the corresponding lower bound on the maximum pole-on breadth, D_{max}, using Eq. (1).

The OC radar albedo, $\hat{\sigma}_{OC}$, of an asteroid is defined to be the ratio of its OC radar cross section (σ_{OC}) to its cross-sectional area,

$$\hat{\sigma}_{OC} = \frac{4\sigma_{OC}}{\pi D_{eff}^2}. \quad (2)$$

$\hat{\sigma}_{OC}$ often varies with rotation and aspect. Published MBA radar albedos vary from a low of 0.039 for the CP-class main-belt Asteroid (MBA) 247 Eukrate (Magri et al., 2007) to a maximum of 0.6 for the M-class 216 Kleopatra (Ostro et al., 2000).

Laboratory studies show that radar albedo is primarily a function of the surface bulk density of the target (Ostro et al., 1985; Garvin et al., 1985). Magri et al. (2007) found that the M-class asteroids have significantly higher radar albedos than all other classes, consistent with the interpretation that they contain a relatively high metal content. Shepard et al. (2008a, 2010) focused exclusively on the M-class and found that about one-third have radar albedos higher than 0.4, a threshold consistent with surface bulk densities of ~3.8 g cm^{-3}, a value expected for iron–nickel with a porosity of ~50%.

The circular polarization ratio, μ_c, is defined to be the ratio of the SC and OC echo power:

$$\mu_c = \frac{\sigma_{SC}}{\sigma_{OC}}. \quad (3)$$

For asteroids, values larger than zero are thought to be caused by wavelength-scale near-surface (~1 m depth for 12 cm wavelength) roughness and inhomogeneities or subsurface multiple scattering. Smooth surfaces have polarization ratios approaching 0.0, while some extremely rough surfaces have values near or at unity (Ostro et al., 2002; Benner et al., 2008).

Benner et al. (2008) reported that all confirmed near-Earth E-class asteroids have high radar circular polarization ratios, with a mean of 0.9. In related work, Shepard et al. (2008b) reported that main-belt E-class Asteroids 44 Nysa and 434 Hungaria also have high circular polarization ratios of 0.50 ± 0.02 and 0.8 ± 0.1, respectively, consistent with the findings of Benner et al. (2008). The causes of this behavior are under investigation, but several hypotheses have been proposed including compositional constraints on near-surface roughness, younger formation or surface ages, and differences in collisional history compared with the other asteroid classes.

3. 64 Angelina

Angelina's diameter is widely reported to be 60 km (e.g. Tedesco, 1989), but the origin of this value is obscure. An occultation in July 2004 with six chords dictates dimensions of 47.6 ± 1.4 km by 53.2 ± 1.7 km, giving an effective diameter of 50.3 ± 1.6 km for that aspect (Shevchenko and Tedesco, 2006).

Angelina's rotation period of 8.752 ± 0.001 h was first reported by Poutanen (1983). Harris et al. (1989) confirmed the period, and noted that the low amplitudes of variation observed at the two viewing aspects, ecliptic longitudes of 124° and 313°, implied a pole direction close to one of those longitudes, and a low ecliptic latitude. Fig. 1 is a plot of the lightcurve amplitudes observed at different ecliptic longitudes (Table 1). Viewing longitudes greater than 180° are plotted (square symbols) at the diametrically opposite longitude, −180° from the observed direction. Also indicated are the longitudes of observation in thermal IR (Morrison and Chapman, 1976), the occultation (Shevchenko and Tedesco, 2006), the longitude of the pole determined by Durech et al. (2011), and the radar observation reported in this paper. The dashed sinusoidal line, not a formal fit but rather a "guide for the eye", implies rather clearly that the direction to the pole (minimum lightcurve amplitude) lies fairly close to 135° longitude (or mirror at 315°), and at low obliquity. Durech et al. (2011) have done a full lightcurve inversion shape and spin orientation model

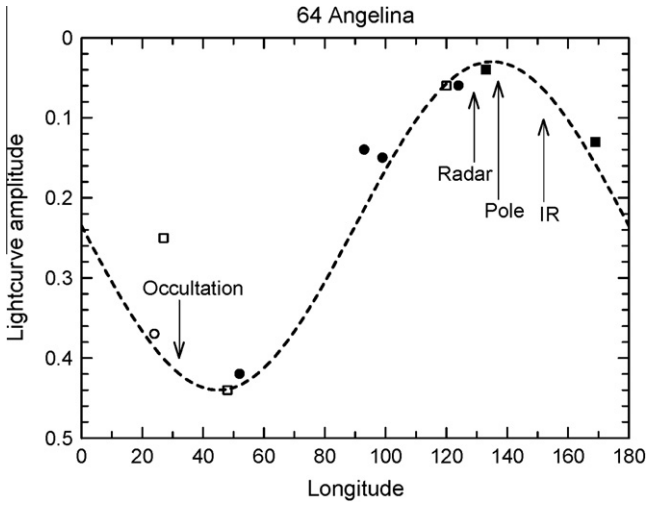

Fig. 1. Plot of lightcurve amplitudes for 64 Angelina vs. the ecliptic longitude of observation. Dashed line is a sinusoidal "fit by eye". Circles are observations plotted at actual observed longitude; squares are plotted −180° from observed longitude; solid symbols are amplitudes from published lightcurves that could be inspected and judged; the open symbols are amplitudes reported in the literature without supporting lightcurves and their quality cannot be judged.

Table 1
Lightcurve amplitudes for 64 Angelina.

Date	λ	Amplitude	Reference
05 December 1978	93	0.13	Poutanen (1983)
08 May 1980	228	0.44	Lagerkvist (1980)
03 August 1981	313	0.04	Harris et al. (1989)
24 January 1988	124	0.05	Harris et al. (1989), Shevchenko et al. (1992)
21 March 1993	207	0.25	Erikson (2000) quoted in Shevchenko et al. (2003)
21 June 1994	300	0.06	Erikson (2000) quoted in Shevchenko et al. (2003)
22 September 1995	24	0.37	Erikson (2000) quoted in Shevchenko et al. (2003)
12 September 1999	349	0.13	Rosenbush et al. (2005)
30 December 2000	99	0.14	Shevchenko et al. (2003)
09 January 2005	52	0.42	Behrend (2011)
17 March 1975	152	IR	Morrison and Chapman (1976)
03 July 2004	38	Occult.	Shevchenko and Tedesco (2006), Durech et al. (2011)
31 January 2010	129	Radar	This paper

Dates are the date of observation, or in some cases opposition dates where observations spanned a range of dates or were not specified.
λ is the ecliptic longitude; it is the longitude of the phase angle bisector for lightcurve observations and IR observations, but geocentric for the occultation and radar observations.
Amplitude is the lightcurve amplitude observed or reported.

Table 2
Observation circumstances.

Asteroid	Date	RA (°)	Dec (°)	λ (°)	β (°)	D (AU)	Runs	SNR
64 Angelina	31 January 2010	132	+18	129	0	1.360	1	10
69 Hesperia	3 February 2010	134	+6	135	−11	1.521	2	24

Positions are mid-epoch for observations.
D is distance from Earth (AU).
Runs is the number of transmit–receive cycles.
SNR is total for each set of observations.

to obtain a unique spin axis of (λ, β) (137°, 14°), and a sidereal rotation period of 8.75032 h. By scaling their model to the 2004 occultation data, they obtain a mean diameter (of a sphere containing the same volume as their polyhedral shape model) of 52 ± 10 km. Using their shape model, we estimate a rough "equivalent ellipsoid" with a = 60 km, b = 53 km, and c = 45 km. This shape results in a polar-view effective diameter (equal area) of $D_{\rm eff}$ = 56 km. This effective diameter, combined with the value H = 7.55 observed in 1981 at near-polar aspect by Harris et al. (1989), yields a visual albedo of $p_{\rm v}$ = 0.54. This is considerably brighter than that reported by Tedesco (1989); the difference is due to a slightly lower (brighter) absolute magnitude (7.55 vs. 7.65) and smaller diameter (56 km vs. 60 km) used in our calculation vs. theirs.

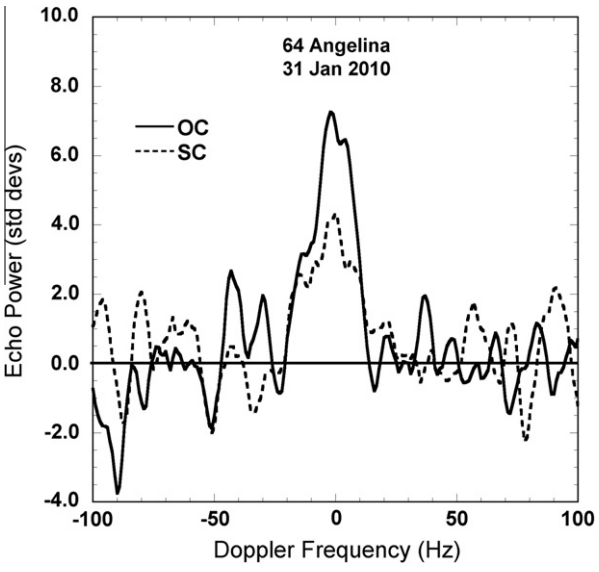

Fig. 2. Continuous wave radar observation of 64 Angelina, smoothed to 8 Hz in frequency.

We obtained one radar run on Angelina on 31 January 2010 (Table 2, Fig. 2). We measured a bandwidth of 35 ± 5 Hz (SNR 10) and an OC radar cross-section of 439 ± 110 km^2 (Table 3). This cross-section and our model (pole-on) diameter give a radar albedo of $\hat{\sigma}_{\rm OC} = 0.18 \pm 0.05$, consistent with those measured for 44 Nysa and 434 Hungaria (Shepard et al., 2008b).

Our measured bandwidth and model size indicates that we were within 12 ± 3° of pole-on. At the time of our observation, Angelina was at (RA, Dec) (132°, 18°) or (λ, β) (129°, 0°) which, assuming the Durech et al. pole, implies a sub-radar latitude of ±74°. Durech et al. do not list formal uncertainties in their pole direction, but given modest values (±5°), we find their model pole, shape, and size and our radar bandwidth constraints to be consistent.

We measured a circular polarization ratio of $\mu_{\rm c}$ = 0.8 ± 0.1, tied for the highest value measured in a main-belt asteroid with 434 Hungaria (Shepard et al., 2008b). As noted earlier, Benner et al. (2008) and Shepard et al. (2008b) noted that all confirmed E-class asteroids, whether near-Earth or main-belt, have exceptionally high polarization ratios.

4. 69 Hesperia

Asteroid 69 Hesperia's rotation rate is 5.6552 h (Torppa et al., 2003). From a single IRAS observation, it has a reported diameter of 138 ± 5 km (Tedesco et al., 2002), while Morrison and Zellner (1979) report a TRIAD (infrared) diameter of 108 km. A single occultation chord of 83 km was obtained in April 2010 (IOTA, www.asteroidoccultation.com). A significant number of lightcurves have been obtained and pole and shape estimates derived from these are listed in Table 4.

We obtained two radar runs on Hesperia on 3 February 2010 (Tables 2 and 3 and Fig. 3). Hesperia was located at (RA, Dec)

Table 3
Radar properties.

Asteroid	Date	Time UT	SNR	ϕ (°)	B (Hz)	σ_{oc} (km^2)	μ_c
64 Angelina	31 January 2010	05:41	10	0	35 ± 5	439	0.77 ± 0.13
69 Hesperia	3 February 2010	04:24	23	0	440 ± 20	5925	0.00 ± 0.04
	3 February 2010	05:21	12	60	310 + 70/−20	2574	0.13 ± 0.04
69 Hesperia	Sum		24	30	440 ± 20	4233	0.05 ± 0.03

Sum is sum of both Hesperia runs. Date and time are mid-epoch of observations.
ϕ is the rotation phase, arbitrarily starting at 0 for first run.
B is zero-crossing bandwidth for data smoothed in frequency (8 Hz for Angelina, 25 Hz for Hesperia).
σ_{oc} is the OC radar cross-section and μ_c is the polarization ratio.

Table 4
Hesperia poles and aspect ratios.

λ (°)	β (°)	a/b	b/c	Source
243 ± 2	+51 ± 4	1.25 ± 0.01	1.45 ± 0.25	D&M (1995)
70 ± 8	−42 ± 9	1.25	1.25	B&R (1998)
244 ± 27	−39 ± 27	1.25	1.25	B&R (1998)
73 ± 5	−45 ± 5	1.1	1.4	Torppa+ (2003)
250	+17	1.27	1.08	Hanus+ (2011)
71	−2	1.27	1.08	Hanus+ (2011)

D&M (1995) is De Angelis and Mottola (1995).
B&R (1998) is Blanco and Riccioli (1998).
Torppa+ (2003) is Torppa et al. (2003).
Hanus+ (2011) is Hanus et al. (2011) and the DAMIT website (http://astro.troja.mff.cuni.cz/projects/asteroids3D/web.php?page=db_asteroid_detail&asteroid_ id=236).
The uncertainty on these poles are reported to be ±10–20°.

(134°, 6°), corresponding to ecliptic (λ, β) (135°, −11°). Based on previously published poles, the sub-radar latitude for these observations is predicted to be 20° (De Angelis and Mottola, 1995), 26° or 7° (Blanco and Riccioli, 1998), 28° (Torppa et al., 2003), or 26–27° (Hanus et al., 2011). For the remaining analyses, we therefore adopt $\delta = 25 \pm 10°$ as the most likely range of sub-radar latitudes.

The results of our radar runs are given in Table 3. We measured bandwidths of 440 ± 20 Hz (run #1, SNR 23; and sum of both runs, SNR 24) and 310 + 70/−20 Hz (run #2, SNR 12), giving an a/b aspect ratio of 1.4 + 0.2/−0.3. This is larger than expected from previous lightcurve-derived aspect ratios (Table 4). However, the left (negative) frequency edge of the second run is quite uncertain and, allowing for this, our results are consistent with all of the a/b ratios derived from lightcurves.

We were undoubtedly close to maximum bandwidth in run #1 (corresponding to a broadside-view of the long or a-axis) because the observed bandwidth dropped considerably in run #2, after 60° of additional rotation. We therefore adopt $B_{max} = 450 + 100/-0$ Hz which recognizes that the maximum bandwidth must be at least as large as we measured and may be considerably higher.

Using our adopted maximum bandwidth ($B_{max} = 450 + 100/-0$ Hz) and sub-radar latitude ($\delta = 25° \pm 10°$), Eq. (1) gives $D_{max} = 100 + 35/-5$ km. Given this diameter and range of uncertainties, we wish to determine: (1) whether our size estimate of Hesperia is at all consistent with the TRIAD and IRAS estimates, and (2) the smallest possible radar albedo consistent with our data. We therefore adopt $D_{max} = 135$ km as the *largest value consistent* with our admittedly sparse dataset, and adopt the axial ratios reported by the latest lightcurve-derived shape (Honus et al., 2011), giving dimensions of 135 km × 106 km × 98 km and $D_{eff} = 110$ km. This estimate is consistent with the TRIAD-based diameter of $D = 108$ km. The IRAS-based $D = 138$ km is inconsistent, but that observation was made when Hesperia was nearly pole-on; our adopted model predicts $D_{apparent} = 120$ km at that aspect, so the discrepancy is reduced somewhat.

Assuming a diameter of $D_{eff} = 110$ km, we estimate a radar albedos of $\hat{\sigma}_{OC} = 0.45 \pm 0.12$ for the sum of all runs, and 0.56 ± 0.14 and 0.27 ± 0.07 for runs 1 and 2 respectively. (We assumed the maximum area dimensions of 135 km × 100 km, for the cross-sectional area in the calculation for run #1.) The radar albedos of run #1 and the sum of all runs are consistent with a surface dominated by high density phases (Shepard et al., 2010), presumably iron–nickel, and are consistent with other high metal M-class asteroids (Mm's). Run #2 has a lower radar albedo, but still much higher than typical for main-belt asteroids (Magri et al., 2007) and also indicates a relatively high bulk density, consistent with significant metal content. We note that every previously observed

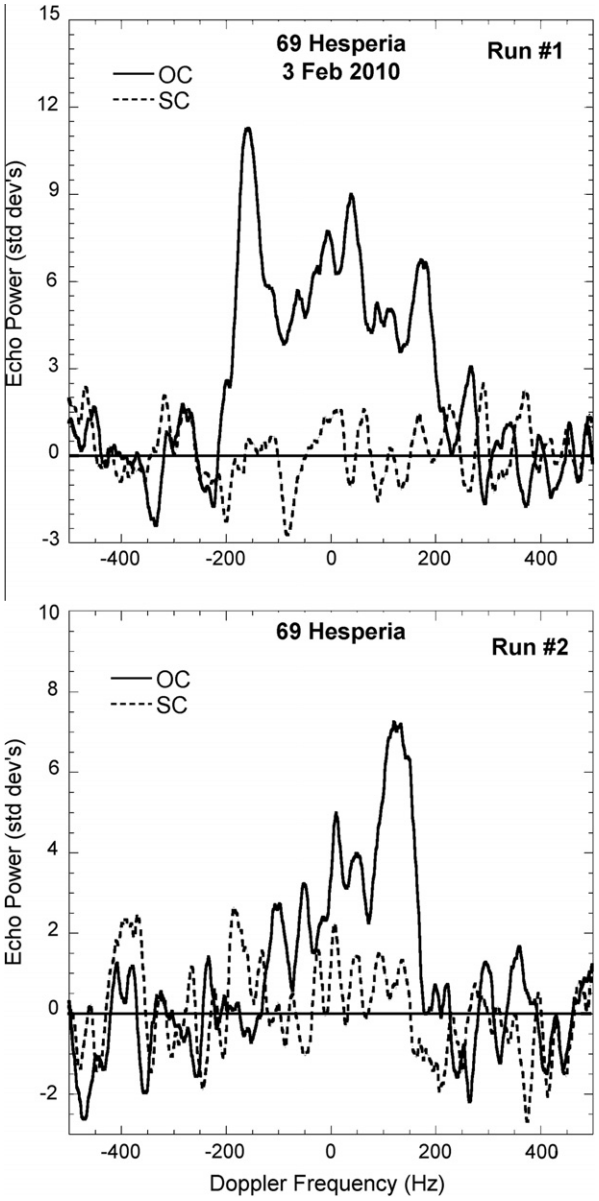

Fig. 3. Continuous wave radar observations of 69 Hesperia, smoothed to 25 Hz in frequency.

Mm-class asteroid shows similar variations in radar albedo with rotation phase; it is hypothesized that these variations are caused by normal shape effects exaggerated by the higher radar albedo of the surface (Shepard et al., 2010).

We measured Hesperia's circular polarization ratio to be $\mu_c = 0.05 \pm 0.05$, indicating a very smooth surface at wavelength scales. This value is consistent with other M-class asteroids, notably several of those with high radar albedos (Shepard et al., 2010).

Even if the IRAS diameter ($D_{eff} = 138$ km) was more accurate than that adopted here, the estimated radar albedo of run #1 is still quite high (0.40) and is also consistent with a high metal content. It therefore seems safe to classify Hesperia as an Mm-class asteroid. With the addition of Hesperia to our sample of 20 M-class asteroids detected with radar, we find that eight (8), or 40%, have high radar albedos and can be classified as Mm, or high metal M-class. The remainder must be dominated by other compositions, most likely enstatite chondrite or other analogue material (Shepard et al., 2010).

5. Summary and conclusions

Radar observations of the E-class Asteroid 64 Angelina are consistent with diameters determined by occultation and thermal infrared and confirm a high optical albedo, consistent with a nearly pure enstatite composition. We also find Angelina to have an unusually high radar polarization ratio, consistent with all other E-class asteroids observed by radar. There are several possible causes for this behavior, but no consensus.

Our observations of M-class 69 Hesperia are consistent with a diameter ~20% smaller than the IRAS estimate and indicate a high radar albedo, suggesting an object dominated by metal phases. When combined with other observations (Shepard et al., 2010), we find that only 40% of M-class asteroids are composed chiefly of metal. This finding may have important implications for models of the origin and evolution of the main asteroid belt.

Acknowledgements

MKS and BEC gratefully acknowledge funding from NSF AST 0908098 and 0908217.The Arecibo Observatory is part of the National Astronomy and Ionosphere Center, which is operated by Cornell University under a cooperative agreement with the National Science Foundation. We thank the technical staff at the observatory for help with observations. Some of this work was performed at the Jet Propulsion Laboratory, California Institute of Technology, under contract with the National Aeronautics and Space Administration. This material is based in part upon work supported by the National Aeronautics and Space Administration (NASA) under the Science Mission Directorate Research and Analysis Programs.

References

Behrend, R., 2011. <http://obswww.unige.ch/~behrend/page1cou.html>.
Bell, J.F., Davis, D.R., Hartmann, W.K., Gaffey, M.J., 1989. Asteroids: The big picture. In: Binzel, R.P., Gehrels, T., Matthews, M.S. (Eds.), Asteroids II. Univ. of Arizona, Tucson, pp. 921–948.
Benner, L.A.M., Ostro, S.J., Magri, C., Nolan, M.C., Howell, E.S., Giorgini, J.D., Jurgens, R.F., Margot, J.L., Taylor, P.A., Busch, M.W., Shepard, M.K., 2008. Near-Earth asteroid surface roughness depends on compositional class. Icarus 198, 294–304.
Blanco, C., Riccioli, D., 1998. Pole coordinates and shape of 30 asteroids. Astron. Astrophys. Suppl. Ser. 131, 385–394.
Chapman, C.R., Salisbury, J.W., 1973. Comparisons of meteorite and asteroid spectral reflectivities. Icarus 19, 507–522.
Clark, B.E. et al., 2004. E-type asteroid spectroscopy and compositional modeling. J. Geophys. Res. 109. doi:10.1029/2003JE002200.
Cloutis, E.A., Gaffey, M.J., Smith, D.G.W., Lambert, R.St.J., 1990. Metal silicate mixtures: Spectral properties and applications to asteroid taxonomy. J. Geophys. Res. 95, 8323–8338.
De Angelis, G., Mottola, S., 1995. Lightcurves and pole determinations for the Asteroids 69 Hesperia, 79 Eurynome and 852 Wladilena. Planet. Space Sci. 43, 1013–1017.
Durech, J., Kaasalainen, M., Herald, D., Dunham, D., Timerson, B., Hanus, J., Frappa, E., Talbot, J., Hayamizu, T., Warner, B.D., Pilcher, F., Galad, A., 2011. Combining asteroid models derived by lightcurve inversion with asteroidal occultation silhouettes. Icarus, in press. doi:10.1016/j.icarus.2011.03.016.
Erikson, A., 2000. The Present Distribution of Asteroid Spin Vectors and its Relevance to the Origin and Evolution of Main Belt Asteroids. Ph.D. Thesis, Berlin.
Gaffey, M.J., 1976. Spectral reflectance characteristics of the meteorite classes. J. Geophys. Res. 81, 905–920.
Gaffey, M.J., Kelley, M.S., 2004. Mineralogical variations among high albedo E-type asteroids: Implications for asteroid igneous processes. Lunar Planet. Sci. XXXV. Abstract #1812.
Gaffey, M.J., McCord, T.B., 1979. Mineralogical and petrological characterizations of asteroid surface materials. In: Gehrels, T. (Ed.), Asteroids. Univ. of Arizona Press, Tucson, pp. 688–723.
Garvin, J.B., Head, J.W., Pettengill, G.H., Zisk, S.H., 1985. Venus global radar reflectivity and correlations with elevation. J. Geophys. Res. 90, 6859–6871.
Hanus, J. et al., 2011. A study of asteroid pole-latitude distribution based on an extended set of shape models derived by the lightcurve inversion method. Astron. Astrophys. 530, A134.
Hardersen, P.S., Gaffey, M.J., Abell, P.A., 2005. Near-IR spectral evidence for the presence of iron-poor orthopyroxenes on the surfaces of six M-type asteroids. Icarus 175, 141–158.
Harris, A.W., Young, J.W., Contreiras, L., Dockweiler, T., Belkora, L., Salo, H., Harris, W.D., Bowell, E., Poutanen, M., Binzel, R.P., Tholen, D.J., Wang, S., 1989. Phase relations of high albedo asteroids: The unusual opposition brightening of 44 Nysa and 64 Angelina. Icarus 81, 365–374.
Lagerkvist, C.-I., 1980. Physical studies of asteroids – An observing programme at ESO. The Messenger 22, 5–7.
Lupishko, D.F., Belskaya, I.N., 1989. On the surface composition of the M-asteroids. Icarus 78, 395–401.
Magri, C., Nolan, M.C., Ostro, S.J., Giorgini, J.D., 2007. A radar survey of main-belt asteroids: Arecibo observations of 55 object during 1999–2003. Icarus 186, 126–151.
Morrison, D., Chapman, C.R., 1976. Radiometric diameters for an additional 22 asteroids. Astrophys. J. 204, 934–939.
Morrison, D., Zellner, B., 1979. Polarimetry and radiometry of the asteroids. In: Gehrels, T. (Ed.), Asteroids. Univ. of Arizona Press, Tucson, pp. 1090–1097.
Ostro, S.J., Campbell, D.B., Shapiro, I.I., 1985. Mainbelt asteroids: Dual polarization radar observations. Science 229, 442–446.
Ostro, S.J. et al., 2000. Radar observations of Asteroid 216 Kleopatra. Science 288, 836–839.
Ostro, S.J. et al., 2002. Asteroid radar astronomy. In: Bottke, W.F., Jr., Cellino, A., Paolicchi, P., Binzel, R.P. (Eds.), Asteroids III. Univ. of Arizona, Tucson, pp. 151–168.
Poutanen, M., 1983. UBV photometry of Asteroid 64 Angelina. In: Lagerkvist, C.I., Rickman, H. (Eds.), Asteroids, Comets, Meteors I. U. Uppsala, Sweden, pp. 45–48.
Rivkin, A.S., Howell, E.S., Lebofsky, L.A., Clark, B.E., Britt, D.T., 2000. The nature of M-class asteroids from 3-μm observations. Icarus 145, 351–368.
Rosenbush, V.K., Kiselev, N.N., Shevchenko, V.G., Jockers, K., Shakhovskoy, N.M., Efimov, Y.S., 2005. Polarization and brightness opposition effects for the E-type Asteroid 64 Angelina. Icarus 178, 222–234.
Shepard, M.K. et al., 2008a. A radar survey of M- and X-class asteroids. Icarus 195, 184–205.
Shepard, M.K., Kressler, K.M., Clark, B.E., Ockert-Bell, M.E., Nolan, M.C., Howell, E.S., Magri, C., Giorgini, J.D., Benner, L.A.M., Ostro, S.J., 2008b. Radar observations of E-class Asteroids 44 Nysa and 434 Hungaria. Icarus 195, 220–225.
Shepard, M.K., Clark, B.E., Ockert-Bell, M., Nolan, M.C., Howell, E.S., Magri, C., Giorgini, J.D., Benner, L.A.M., Ostro, S.J., Harris, A.W., Warner, B.D., Stephens, R.D., Mueller, M., 2010. A radar survey of M- and X-class asteroids II. Summary and synthesis. Icarus 208, 221–237.
Shevchenko, V.G., Tedesco, E.F., 2006. Asteroid albedos deduced from stellar occultations. Icarus 184, 211–220.
Shevchenko, V.G., Chiornu, V.G., Krugly, Yu.N., Lupishko, D.F., Mohamed, R.A., Velichko, F.P., 1992. Photometry of seventeen asteroids. Icarus 100, 295–306.
Shevchenko, V.G., Krugly, Y.N., Chiorny, V.G., Belskaya, I.N., Gaftonyuk, N.M., 2003. Rotation and photometric properties of E-type asteroids. Planet. Space Sci. 51, 525–532.
Tedesco, E.F., 1989. Asteroid magnitudes, UBV colors, and IRAS albedos and diameters. In: Binzel, R.P., Gehrels, T., Matthews, M.S. (Eds.), Asteroids II. Univ. of Arizona, Tucson, pp. 1090–1138.
Tedesco, E.F., Noah, P.V., Noah, M., 2002. The supplemental IRAS minor planet survey. Astron. J. 123, 1056–1085.
Tholen, D., 1984. Asteroid Taxonomy from Cluster Analysis of Photometry. Ph.D. Thesis, Univ. of Arizona, Tucson, 150pp.
Torppa, J., Kaasalainen, M., Michalowski, T., Kwiatkowski, T., Kryszczynska, A., Denchev, P., Kowalski, R., 2003. Shapes and rotational properties of thirty asteroids from photometric data. Icarus 164, 346–383.
Vernazza, P., Brunetto, R., Binzel, R.P., Perron, C., Fulvio, D., Strazzulla, G., Fulchignoni, M., 2009. Plausible parent bodies for enstatite chondrites and mesosiderites: Implications for Lutetia's fly-by. Icarus 202, 477–486.
Vilas, F., 1994. A cheaper, faster, better way to detect water of hydration on Solar System bodies. Icarus 111, 456–467.
Zellner, B., Leake, M., Morrison, D., Williams, J.G., 1977. The E-asteroids and the origin of the enstatite chondrites. Geochim. Cosmochim. Acta 41, 1759–1767.